Published in "Journal of Geophysical Research 117: F04010, 2012"
which should be cited to refer to this work.

Distributed ice thickness and volume of all glaciers around the globe

Matthias Huss[1] and Daniel Farinotti[2,3]

[1] A new physically based approach for calculating glacier ice thickness distribution and volume is presented and applied to all glaciers and ice caps worldwide. Combining glacier outlines of the globally complete Randolph Glacier Inventory with terrain elevation models (Shuttle Radar Topography Mission/Advanced Spaceborne Thermal Emission and Reflection Radiometer), we use a simple dynamic model to obtain spatially distributed thickness of individual glaciers by inverting their surface topography. Results are validated against a comprehensive set of thickness observations for 300 glaciers from most glacierized regions of the world. For all mountain glaciers and ice caps outside of the Antarctic and Greenland ice sheets we find a total ice volume of $170 \times 10^3 \pm 21 \times 10^3$ km^3, or 0.43 ± 0.06 m of potential sea level rise.

1. Introduction

[2] Mountain glaciers and ice caps are expected to contribute significantly to sea level rise over the next decades [*Meier et al.*, 2007; *Radić and Hock*, 2011]. However, the volume of these almost 200,000 glaciers, and thus their potential sea level equivalent, are still poorly known. Physically based methods for calculating ice thickness distribution have been applied to small subsets of glaciers [e.g., *Farinotti et al.*, 2009a; *Li et al.*, 2012], but not at larger scales. To date, global fresh water volume stored in glaciers and ice caps has only been estimated using statistical volume-area scaling [*Chen and Ohmura*, 1990; *Bahr et al.*, 1997]. Relations between glacier area and volume do, however, not account for other characteristics of individual glaciers, e.g., their surface geometry and local climate, and therefore are subject to considerable uncertainties [*Haeberli and Hoelzle*, 1995; *Cogley*, 2012]. Furthermore, scaling does not yield any information on the spatial distribution of ice thickness, which is required for the dynamical component of any model aiming, for example, at simulating future cryospheric contributions to sea level rise, or changes in the hydrology of glacierized mountain ranges.

[3] Ground penetrating radar (GPR) is a well established technique to measure ice thickness, but is laborious and only applicable to individual glaciers [e.g., *Nolan et al.*, 1995; *Dowdeswell et al.*, 2002]. Recently, several methods to calculate basal glacier topography based on surface characteristics have been developed [*Farinotti et al.*, 2009b; *Clarke et al.*, 2009; *Li et al.*, 2012; *Linsbauer et al.*, 2012], but the applicability of these methods at the worldwide scale at the time of their development was hampered by the unavailability of the required data input (e.g., flow lines), and/or computational resources. The few global glacier volume estimates available today [e.g., *Dyurgerov and Meier*, 2005; *Radić and Hock*, 2010] are all based on volume-area scaling. Excluding glaciers and ice caps around Greenland and Antarctica they range from 0.24 ± 0.03 m of global sea level equivalent (SLE) [*Raper and Braithwaite*, 2005] to 0.41 ± 0.03 m SLE [*Radić and Hock*, 2010]. The entire glacier volume outside of the two ice sheets is quantified as 0.60 ± 0.07 m SLE by *Radić and Hock* [2010].

[4] Here, we propose and apply a new approach for calculating volume and thickness distributions of all glaciers worldwide which allows adding the third dimension to glacier inventory data. By combining glacier outlines from the almost globally complete Randolph Glacier Inventory [*Arendt et al.*, 2012] with digital elevation models (DEMs), we calculate glacier-specific distributed thickness based on an inversion of surface topography using the principles of flow dynamics. We present the first global estimate of glacier ice volume using a physically based method that individually considers the characteristics of each glacier.

2. Data

[5] The Randolph Glacier Inventory (RGI) is the first complete data set containing outlines of almost all glaciers and

[1]Department of Geosciences, University of Fribourg, Fribourg, Switzerland.
[2]Laboratory of Hydraulics, Hydrology and Glaciology, ETH Zurich, Zurich, Switzerland.
[3]Now at Section 5.4, Hydrology, GFZ German Research Centre for Geosciences, Potsdam, Germany.

Corresponding author: M. Huss, Department of Geosciences, University of Fribourg, Chemin du Musée 4, CH-1700 Fribourg, Switzerland. (matthias.huss@unifr.ch)

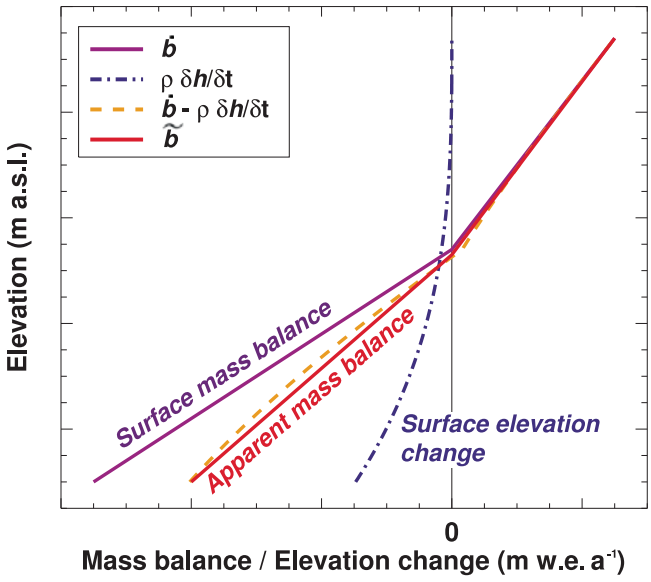

Figure 1. Schematic representation of the altitudinal distribution of surface mass balance $\dot{b}$, hypothetical elevation change $\rho\partial h/\partial t$, and apparent mass balance $\tilde{b}$ over the glacier using linear elevation gradients (approximating $\dot{b} - \rho \cdot \partial h/\partial t$, see equation (1)).

ice caps other than the two ice sheets [*Arendt et al.*, 2012]. The RGI is a recent community effort that builds on the glacier shapes already in the Global Land Ice Measurement from Space (GLIMS) database [*Raup et al.*, 2007], which is extended using new satellite imagery and, in some regions, glacier outlines digitized from topographical maps. The RGI is a provisional data set; that is, it has not been extensively quality checked, and in most regions there is a lack of information on the date and the source of imagery used to produce the outlines. Nearly all regions include glaciers delineated by individual catchments, but for parts of some regions (Alaska, Antarctic and Subantarctic, central Asia, Greenland periphery, low latitudes, New Zealand, Scandinavia and southern Andes) only polygons of glacier complexes are provided. The inventory is divided into 19 regions (Figure S1 in Text S1 in the auxiliary material) that are similar to those defined by *Radić and Hock* [2010].[1] We use the RGI version 2.0 that was released in June 2012 [*Arendt et al.*, 2012].

[6] The separation of glaciers and ice caps from the ice sheet in Greenland and Antarctica is still open to debate [e.g., *Rastner et al.*, 2012]. The RGI includes some ice caps that are connected with the ice sheet in their accumulation areas; the Antarctic mainland is not contained in the RGI. Here, we use all outlines provided by the RGI v2.0.

[7] Several Earth-covering DEMs allow extracting spatially distributed topographical attributes for arbitrary glaciers based on inventory data [*Frey and Paul*, 2012]. Between 60°N and 60°S we use the hole-filled Version 4 Shuttle Radar Topography Mission (SRTM) DEM with a resolution of about 90 m retrieved from *srtm.csi.cgiar.org* [*Jarvis et al.*, 2008]. North and south of 60° the Advanced Space-borne Thermal Emission and Reflection Radiometer (ASTER) Global DEM Version 2 (about 30 m resolution) provided by NASA is used. Elevation uncertainty in both DEMs is estimated as ±10–20 m for mountain areas [e.g., *Fujita et al.*, 2008]. The ASTER DEM is however affected by some gaps and erroneous data, particularly in the accumulation areas of ice caps.

[8] A comprehensive set of ice thickness observations with at least one data point for every RGI region has been compiled from more than 70 publications (Table S1 in Text S1). We extend the sample of published measurements of mean glacier thickness previously used for the calibration of volume-area scaling relations [e.g., *Bahr et al.*, 1997] by including direct information on point ice thickness mostly based on GPR profiles. The point thicknesses are assumed to be more accurate as they are not affected by the uncertainty of extrapolation. In total, we use average ice thickness data for 218 and point thickness measurements for 87 glaciers to validate our results.

3. Methods

[9] The method to compute ice thickness distribution is based on glacier mass turnover and ice flow mechanics and further develops the approach presented by *Farinotti et al.* [2009b]. We estimate surface mass balance distribution, calculate the volumetric balance flux and convert it into thickness using the flow law for ice [*Glen*, 1955]. Required input data are limited to glacier outlines and a DEM: both are readily available from the RGI and SRTM/ASTER data for almost 200,000 glaciers worldwide.

[10] First, SRTM/ASTER DEMs are interpolated to a regular grid covering the glacier. The spatial resolution depends on glacier size and is 25–200 m. This DEM is intersected with the glacier outline, providing area S_i and mean slope $\overline{\alpha}_i$ for glacier surface elevation band i. Vertical spacing of elevation bands is dz = 10 m. Width w_i of each elevation band is obtained with $w_i = S_i/l_i = S_i \cdot \tan(\overline{\alpha}_i)/dz$. l_i is the horizontally projected length of the elevation band. Thus, the three-dimensional geometry is reduced to glacier characteristics distributed over the altitudinal range. All calculations are performed using this simplified 2-D shape of the glacier.

[11] In order to conserve mass, surface mass balance $\dot{b}$ must be balanced by ice flux divergence and the surface elevation change $\partial h/\partial t$. Following [*Farinotti et al.*, 2009b], $\dot{b}$ and $\partial h/\partial t$ are lumped into a new variable, the 'apparent mass balance' $\tilde{b}$ defined as

$$\tilde{b} = \dot{b} - \rho \cdot \partial h/\partial t, \tag{1}$$

where ρ is the ice density. This has the advantage that estimating the distribution of $\tilde{b}$ over the glacier allows direct calculation of the balancing ice volume flux, even if the observed glacier surface does not correspond to a steady state geometry (Figure 1). The quantity of the apparent mass balance is similar to that of the ice emergence velocity [*Cogley et al.*, 2011] and, in our case, does not refer to a specific period in time.

[12] The apparent mass balance distribution is calculated using two altitudinal gradients $d\tilde{b}/dz_{\mathrm{abl}}$ and $d\tilde{b}/dz_{\mathrm{acc}}$ for the ablation and the accumulation area, respectively [*Farinotti*

[1] Auxiliary materials are available in the HTML. doi:10.1029/2012JF002523.

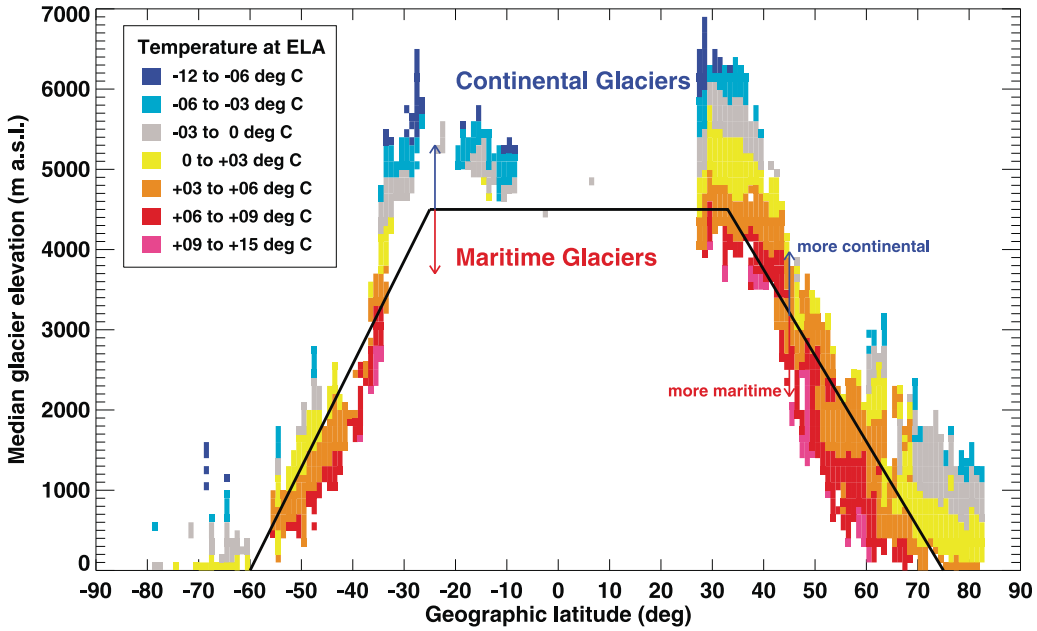

Figure 2. Air temperature of the warmest month according to the NCEP reanalysis at the median glacier elevation ELA_g (modified after *Cogley* [2012] with permission from Elsevier). The solid line shows the reference latitude-dependent ELA, ELA_{lat}, corresponding to average continentality ($C = 1$), following a maximum monthly temperature of +3°C at the ELA.

et al., 2009b]. We assume them to be linearly related by a constant factor $f_{db/dz} = 0.55$ with smaller gradients in the accumulation area. Accumulation rates are limited to $\widetilde{b}_{max}$ in order to prevent unrealistically high accumulation on glaciers with a large elevation range. $\widetilde{b}_{max}$ corresponds to the apparent mass balance 700 m above the equilibrium line altitude (ELA).

[13] For glaciers smaller than a critical area $S_{crit} = 25$ km^2, $d\widetilde{b}/dz$ is decreased linearly with glacier area to a minimum value of $d\widetilde{b}/dz_{min}$ for glacier sizes <0.05 km^2. This reduction in apparent mass balance gradient is necessary to account for the particular combination of $\dot{b}$ and $\partial h/\partial t$ in the distribution of apparent mass balance $\widetilde{b}$ of small glaciers (equation (1)): A snow patch with no flow dynamics, an object at the small end of the glacier size continuum, will respond to a shift in climate forcing with a change in surface lowering only. $\dot{b}$ then equals $\rho\partial h/\partial t$, and $\widetilde{b}$ (and thus $d\widetilde{b}/dz$) is zero (see also Figure 1). On the other hand, large glaciers will react with a change in flow but relatively limited elevation change over much of their altitudinal range [*Jóhannesson et al.*, 1989]. Therefore, $\dot{b}$ approximately corresponds to $\widetilde{b}$, and $d\widetilde{b}/dz$ is close to mass balance gradients observed in the field [e.g., *Hoelzle et al.*, 2003].

[14] Maritime glaciers have balance gradients that are considerably higher than those of continental glaciers [e.g., *Oerlemans and Fortuin*, 1992]. In order to include this effect in the estimation of glacier-specific $d\widetilde{b}/dz$, we estimate continentality of each glacier based on the RGI data. We define a simple relation between geographical latitude and a reference ELA (see Figure 2) corresponding to neither particularly maritime nor particularly continental conditions using air temperature at the actual glacier ELA as a proxy for continentality: high temperatures indicate high accumulation rates, and low temperatures indicate dry conditions. Ground surface air temperature is taken from the NCEP reanalysis [*Kalnay et al.*, 1996] and is scaled with a lapse rate of -6.5°C km^{-1} to the altitude of each RGI glacier (Figure 2). With the latitude-dependent reference ELA, ELA_{lat}, and the median altitude ELA_g of each RGI glacier, a continentality index C is obtained as

$$C = \left(\frac{ELA_{lat} - ELA_g}{f_{cont}} + 1\right), \quad (2)$$

where $f_{cont} = 2400$ m is a constant parameter that is calibrated to observed differences in mass balance gradients between continental and maritime glaciers [*World Glacier Monitoring Service* (*WGMS*), 2008]. The observed range of $ELA_{lat} - ELA_g$ is from –880 m to +1580 m (2.5% and 97.5% quantiles). C is used to adapt the reference apparent surface mass balance gradient $d\widetilde{b}/dz_0$ to local conditions

$$d\widetilde{b}/dz = d\widetilde{b}/dz_0 \cdot C. \quad (3)$$

[15] For each glacier, apparent mass balance distribution is computed using the gradients $d\widetilde{b}/dz_{abl}$ and $d\widetilde{b}/dz_{acc}$ with the ELA that yields a balanced mass budget, i.e., $\int_S \widetilde{b} \cdot ds = 0$ (restrictions for tidewater glaciers, see below). The volumetric balance flux for each elevation band i of the glacier is then obtained by integration of $\widetilde{b}$ along the glacier (Figure 3a).

[16] Inversion of ice volume flux to obtain ice thickness using Glen's flow law (only ice deformation) needs to

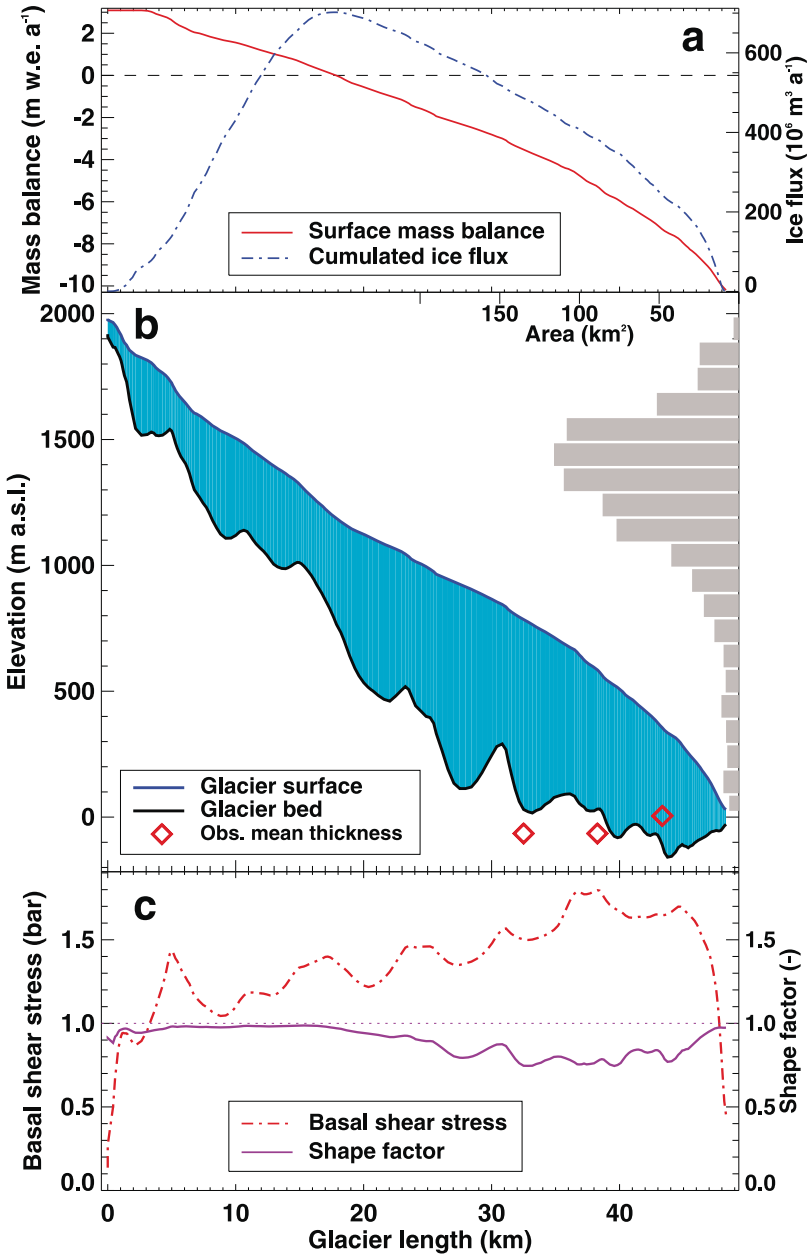

Figure 3. Longitudinal profile with derived variables for Taku Glacier (Alaska). (a) Estimated apparent surface mass balance and corresponding ice volume flux. (b) Glacier surface and calculated bedrock elevation using elevation band thickness. Observed mean thickness at cross profiles [*Nolan et al.*, 1995] is indicated by diamonds. Glacier area in 100 m elevation bands is shown by bars. (c) Inferred basal shear stress τ and shape factor F_s along the glacier.

account for the fact that an important fraction of flux can be due to sliding at the glacier base. Therefore, we correct calculated volumetric balance fluxes derived from the apparent surface mass balance distribution for basal sliding. Volumetric flux is multiplied by $(1 - f_{sl})$, a factor assumed to be constant along the glacier. f_{sl} varies between 0 and 0.55, is glacier-specific, and is calculated as

$$f_{sl} = c_1 + c_2 \cdot (S - 10) + c_3 \cdot (C - 1), \quad (4)$$

where $c_1 = 0.2$, $c_2 = 0.1$, $c_3 = 4$ are constants, S is the glacier area (km^2) and C is continentality (equation (2)). The area-dependent term $c_2(S - 10)$ is restricted to the range $[-0.1, 0.1]$, and the continentality term $c_3(C - 1)$ to $[-0.25, 0.25]$. Our purely empirical sliding parameterization aims at roughly capturing glacier- and region-specific differences in basal sliding which are difficult to constrain at the global scale. Studies estimating the fraction of sliding relative to total glacier flow [e.g., *Paterson*, 1970, and references therein] provide some verification.

[17] Quantifying the calving flux of tidewater glaciers is a challenge as glacier surface geometry derived from a DEM only allows a general statement about the possibility of ice loss by calving (glacier in contact with ocean), but not about

its magnitude. We account for the calving flux of large water-terminating glaciers by reducing the ELA that yields a balanced surface mass budget by a value Δ ELA$_{calv}$ which is separately defined for each RGI region but is not glacier-specific. Ice flux calculated from surface mass balance thus becomes >0 at the glacier terminus. This correction mimics calving and results in an increase in ice flux. The number of glaciers of which we find the possibility for a considerable calving flux is relatively limited (a dozen to a few hundred per region). However, these glaciers dominate their regions in terms of surface area (and volume), and the proportion of calving glaciers is higher than 50% for, e.g., peripheral Greenland and Antarctica, Arctic Canada and the Russian Arctic. Δ ELA$_{calv}$ is poorly constrained, and we estimate values of between 30 m and 250 m. Calculated calving fluxes were compared to published values for Arctic ice caps [*Dowdeswell et al.*, 2002; *Hagen et al.*, 2003; *Williamson et al.*, 2008] indicating an agreement within 50%.

[18] Using an integrated form of Glen's flow law [*Glen*, 1955], the ice thickness h_i for every elevation band i is calculated as

$$h_i = \sqrt[n+2]{\frac{(1-f_{sl})\cdot q_i}{2A_f(T)}\cdot\frac{n+2}{\left(F_{s,i}\rho g\sin\overline{\alpha_i}\right)^n}}, \quad (5)$$

with q_i the ice flux normalized by glacier width, f_{sl} a factor accounting for basal sliding (equation (4)), $n = 3$ the exponent of the flow law, ρ the ice density, g the acceleration of gravity, and $F_{s,i} = w_i/(2h_i + w_i)$ a valley shape factor [*Nye*, 1965]. As h enters the calculation of F_s, Equation 5 is solved iteratively. The rate factor of the flow law, $A_f(T)$, is assumed to be 0.075 bar^{-3} yr^{-1} for temperate glaciers (englacial temperature of ≈0°C) [e.g., *Gudmundsson*, 1999]. A dependence of A_f on ice temperature is evident yielding lower values for polythermal and cold glaciers [*Cuffey and Paterson*, 2010]. We estimate the englacial temperature of each glacier by assuming a constant temperature offset between glacier-average ice temperature and mean annual air temperature at the ELA (given by the NCEP reanalysis) of $\Delta T_{ice-air}$ = 7°C [*Huang*, 1990]. For nontemperate glaciers, A_f is reduced with ice temperature T using a constant factor $f_{A(T)}$ = 7°C as

$$A_f(T) = A_f(T=0)\cdot\frac{f_{A(T)}}{f_{A(T)}-T}. \quad (6)$$

We are aware that our approach for estimating a temperature-dependent flow rate factor A_f is crude but consider it as a first order approximation that is essential to our approach for polythermal and cold glaciers and ice caps.

[19] According to *Kamb and Echelmeyer* [1986] the basal shear stress $\tau_i = (F_{s,i}\rho g h_i \sin\alpha_i)$ should be smoothed over a distance of 10–20 times the local ice thickness in order to account for the influence of longitudinal stress gradients on glacier flow. Therefore, τ is smoothed accordingly and reintroduced into equation (5). Convergence for h, F_s and τ is reached after fewer than 10 iterations.

[20] These operations provide mean ice thickness in 10 m elevation bands along a longitudinal glacier profile (Figure 3).

[21] As a last step, the mean elevation band thicknesses h_i are extrapolated from the simplified 2-D shape of the glacier to a regular grid using a scheme that inversely weights the distance to the closest glacier boundary point and attaches a weight proportional to $(\sin\alpha)^{n/(n+2)}$ (based on equation (5)) to the surface slope α of each grid cell. As $1/\sin\alpha$ tends to infinity for small α, local slopes are constrained to exceed a threshold $\alpha_{cutoff} = 6°$ [*Farinotti et al.*, 2009b]. The extrapolation scheme conserves elevation band ice volume. Gridded ice thickness is finally smoothed in order to remove local noise originating from surface roughness. The extrapolation procedure results in an estimate of ice thickness for each grid cell of every glacier (Figure 4).

4. Uncertainty Assessment

[22] The apparent mass balance gradient is the primary parameter in need of calibration and was constrained by tuning calculated thickness to high-quality GPR profiling data for 21 glaciers in the Swiss Alps [see, e.g., *Farinotti et al.*, 2009a]. An optimized value of $\widetilde{db}/dz_{abl,0} = 5.5 \times 10^{-3}$ meters water equivalent (mwe) m^{-1} is found. Other model parameters are based on literature values, or were constrained based on independent observations of the related processes. We use the same parameter set that accounts for glacier-specific variations due to continentality and ice temperature for individually calculating ice thickness distribution of all glaciers in every glacierized region of the world (see Table S2 in Text S1 for a complete list of model parameter values).

[23] We directly compare our values of $\widetilde{db}/dz$ to observed mass balance gradients for 44 glaciers [*WGMS*, 2008] on all continents. On average, $\widetilde{db}/dz$ is 22% lower than the observed gradients ($6.2 \pm 1.9 \times 10^{-3}$ mwe m^{-1}) which is reasonable given the definition of the apparent mass balance gradient, and the observation that most glaciers have been losing mass in recent decades [*WGMS*, 2008]. Our parameterization of continentality (equation (2)) reproduces the observed regional variability in mass balance gradients with a root-mean-square error of 1.5×10^{-3} mwe m^{-1}.

[24] Validation of simulated ice thickness against the complete set of published thickness data is shown in Figure 5. Comparison of calculated h_{calc} and measured h_{meas} ice thickness of individual glaciers is performed for (1) average ice thickness h_{avg} and (2) point thickness h_p. For the latter, all available point thickness observations (mostly from GPR profiles), and corresponding calculated thicknesses for the same locations, are arithmetically averaged providing one value h_p per glacier. The overall bias in ice thickness given by the difference between the average of all calculated and measured thicknesses ($\overline{h_{calc}} - \overline{h_{meas}}$) is 0 m for mean thickness, and 10 m for point thickness. The root-mean-square of the relative single-glacier error ($|(h_{calc} - h_{meas})|/h_{meas}$) is around 30% and includes uncertainties in (1) the thickness modeling, (2) the glacier outlines and the DEM used, and (3) the field data (GPR resolution, extrapolation, inconsistency of measurement date and inventory date).

[25] Given the limited data input and the degree of simplification in our approach, the agreement for different glacier types and regions is satisfying, although the mismatch can be significant for individual glaciers (Figure 5). An

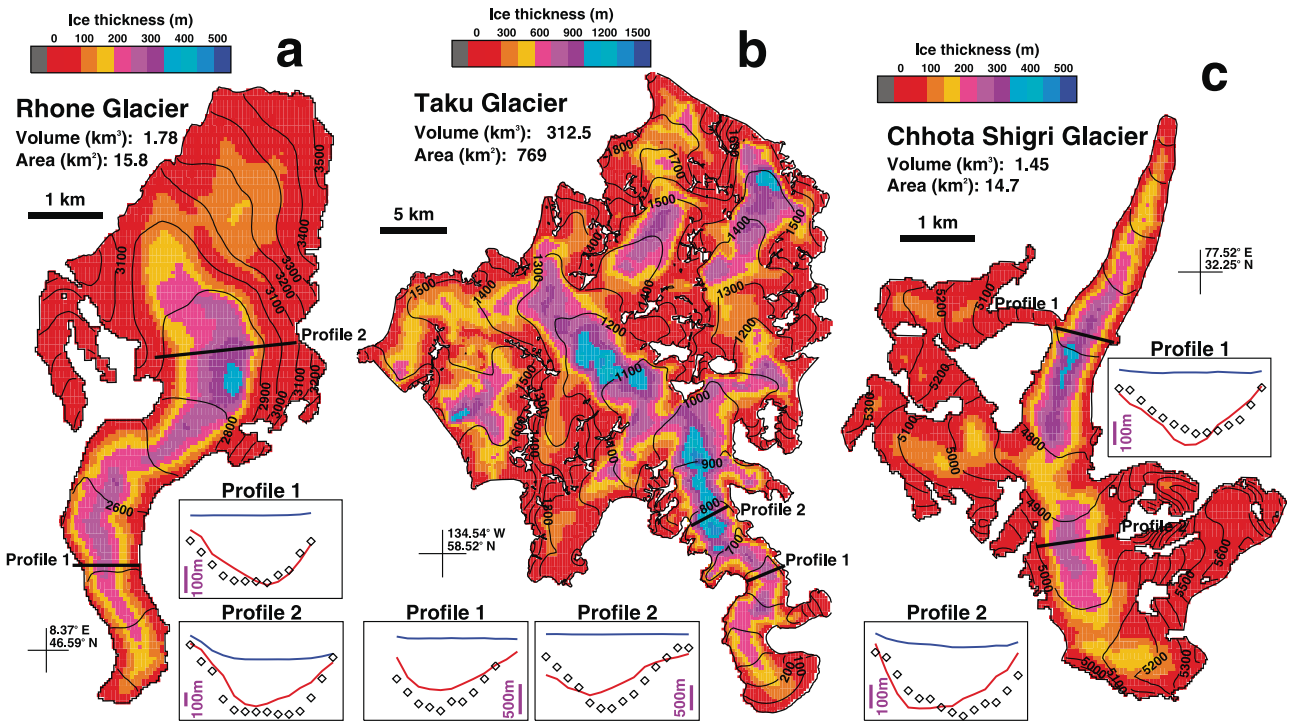

Figure 4. Calculated ice thickness distribution of (a) Rhone Glacier (European Alps), (b) Taku Glacier (Alaska), and (c) Chhota Shigri Glacier (Himalaya). Note that for Taku the scale differs from that for Rhone and Chhota Shigri. Selected profiles with measured (diamonds) and calculated (red line) ice thicknesses are shown in the insets (view in direction of flow, arbitrary scale). The blue line represents the glacier surface. Data are based on GPR surveys [*Farinotti et al.*, 2009b; *Nolan et al.*, 1995; *Azam et al.*, 2012].

underestimation for glaciers with thicknesses of 30–70 m is evident. This bias originates from the almost 80 glaciers with published measurements of mean thickness in north and central Asia [e.g., *Macheret et al.*, 1988]. The differences are likely explained in part by inaccurate georeferencing of the glacier shapes in that region, leading to errors in glacier surface topography (overestimation of surface slope and thus too small thickness) when intersecting them with a DEM. Due to the paucity of validation data, the performance of our method for ice caps is difficult to judge. Based on published ice cap volumes (Table S1 in Text S1) we presume that our method is suitable for estimating mean ice thickness although the quality of calculated ice cap thickness distribution is inferior to that of mountain glaciers.

[26] In order to provide a confidence interval for our global ice volume estimate, we assess all quantifiable uncertainties. The accuracy of calculated ice thickness is affected by (1) the estimation uncertainty in the parameters and the simplifications in the modeling, (2) the uncertainty in the SRTM/ASTER DEM, and (3) the uncertainty in glacier shapes provided by the RGI. Each of these sources of uncertainty is separately assessed for every region based on sensitivity studies. We do not use the set of ice thickness data (Figure 5) for assessing the errors in regional/global ice volume as the spatial distribution of the measurements is not representative, and they might themselves be subject to considerable uncertainties.

[27] The various assumptions and parameterizations in our model have an important impact on the results. We perform a set of sensitivity experiments to quantify a possible bias in global ice volume arising from parameter uncertainty. All parameters used in the modeling were individually varied within plausible ranges. The five most sensitive parameters were discerned and physically reasonable bounds of uncertainty were defined (Table 1). The volume of all RGI glaciers is recalculated by individually varying each of the five important parameters between a maximum and a minimum value. For single-parameter uncertainties, we find an ice volume sensitivity of between ±0.6% and ±4.6% compared to the global volume obtained with the reference parameter set (Table 1). Total ice volume uncertainty σ_M due to poorly constrained parameter values is evaluated by combining the individual uncertainties σ_p, assumed to be independent, using error propagation as $\sigma_M = \left(\sum_{i=1}^{5} \sigma_{p,i}^2\right)^{0.5}$. σ_M is ±6–11% for individual RGI regions (Table S3 in Text S1).

[28] We estimate the impact of inaccurate elevation data on calculated ice thickness by artificially perturbing the surface topography of selected glaciers within the uncertainty ranges of the SRTM/ASTER DEM [*Fujita et al.*, 2008; *Frey and Paul*, 2012]. The effect of a constant or altitudinal bias in the DEM is negligible (<0.5% difference in ice volume). Large but spatially localized errors and data gaps, mainly restricted to high-latitude ice cap accumulation areas (ASTER DEM), can however strongly affect computed thickness of individual glaciers by ±5–25%. Based on regional elevation data quality and sensitivity tests, we estimate a relative uncertainty σ_{DEM} due to erroneous DEM

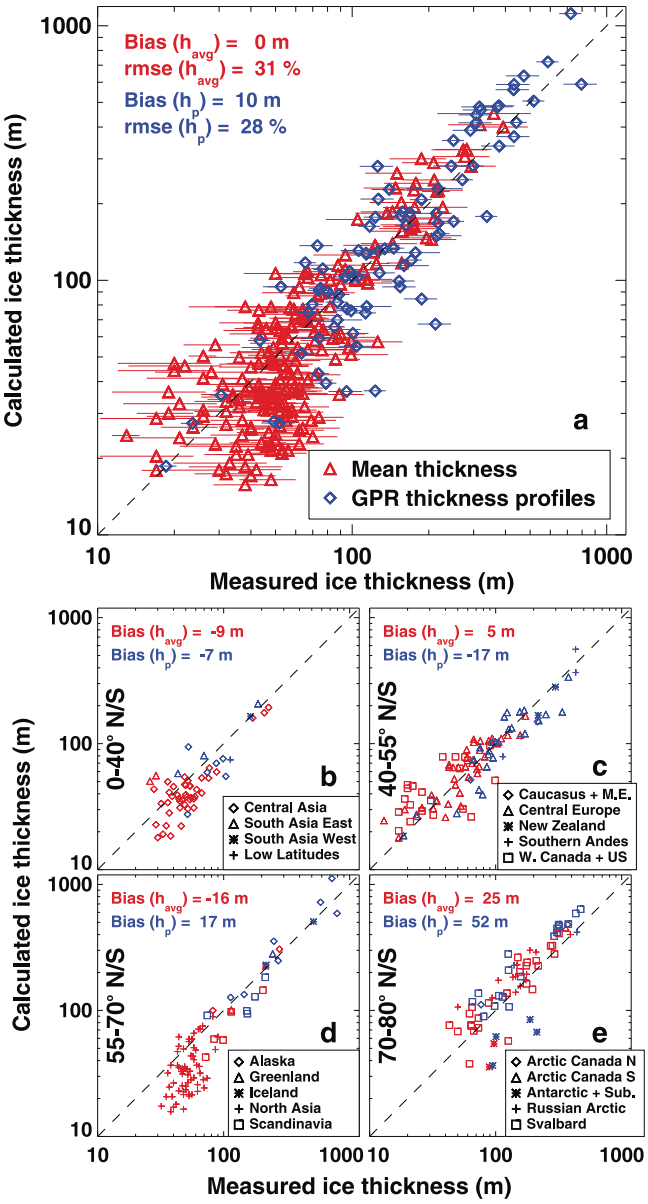

Figure 5. (a) Validation of calculated ice thickness with direct observations. Red triangles refer to published values of mean thickness h_{avg}, blue diamonds show single-glacier means h_p of point-to-point comparisons to ice thickness measurements. Estimated uncertainties in the thickness data are shown by bars. Note that both axes are logarithmic. The bias and the root-mean-square error (RMSE) are given. (b–e) Same as Figure 5a but specified for groups of regions assembled according to their latitude. M.E., Middle East.

data for each RGI region individually (Table S3 in Text S1). σ_{DEM} is assumed to be as low as ±1% in eight regions, but ±20% in the Antarctic and Subantarctic.

[29] Uncertainties in the glacier outlines provided by the RGI control calculated thicknesses in various ways. The quality of the glacier outlines depends on the source and the date of inventory, as well as on the accuracy of the digitization. Most regions are covered by relatively recent satellite imagery, but some glacier shapes also originate from topographical maps that are several decades old [*Arendt et al.*, 2012]. The impact of inaccurate outlines can be significant and needs to be assessed at the single-glacier scale. The georeferencing of the glacier shapes is crucial to the applicability of our approach. A shift relative to the underlying DEM results in errors in glacier hypsometry, and most significantly a bias toward too small ice thickness due to steeper surface slopes. According to sensitivity tests, georeferencing errors of 200 m cause ice volume uncertainties of 1–10% depending on glacier size and slope.

[30] For some regions, the RGI only provides polygons for glacier complexes, which can contain dozens of individual glaciers. As we employ a spatially distributed approach (see, e.g., Figure 4) we can cope with glacier complexes with only a minor loss in accuracy. The performance for reproducing glacier complex volume is validated for the RGI region Arctic Canada South (40,893 km^2), and the Aletsch region (250 km^2), Swiss Alps, for which both single-glacier shapes and polygons for glacier complexes are available. Regional ice volume decreases by 7% in Arctic Canada South and 4% in the Alps, when single-glacier outlines are used instead of glacier complexes.

[31] Based on the assessment of the above factors, and their relative regional importance, we arbitrarily assign estimated uncertainties σ_{DEM} depending on the DEM accuracy, and σ_{RGI} referring to uncertainties in the RGI shapes to each region (Table S3 in Text S1). The overall uncertainty σ_V in calculated regional and global ice volume is then obtained by combining the individual error sources with

$$\sigma_V = \sqrt{\sigma_M^2 + \sigma_{DEM}^2 + \sigma_{RGI}^2}, \quad (7)$$

where σ_M is the uncertainty from model parameters. We find a total uncertainty of our global ice volume estimate of ±12%.

5. Results and Discussion

[32] We evaluated 171,000 glaciers and ice caps around the globe. For each glacier, gridded thickness distribution, and ice volume were computed, as were surface slope, the valley shape factor and basal shear stress along the glacier. Figures 3 and 4 show illustrative results of calculated thickness distribution for selected glaciers.

[33] We compute a total volume of all glaciers and ice caps other than the two ice sheets of 170 × 10^3 ± 21 × 10^3 km^3. Assuming an ice density of 900 kg m^{-3} and an ocean area of 362.5 × 10^6 km^2 [*Cogley et al.*, 2011] this corresponds to 0.43 ± 0.06 m of potential global sea level rise (Table 2). One third of the glacier volume is located in peripheral Greenland and Antarctica. This number is, however, relatively uncertain and might be subject to changes depending on the separation of ice caps from the ice sheets in the inventories. The volume of glaciers outside of Greenland and Antarctica is 114 × 10^3 ± 11 × 10^3 km^3, or 0.29 ± 0.03 m SLE. The distribution of glacier ice volume is dominated by Arctic ice caps with a relatively large mean thickness; more than 40% of global volume is concentrated in the Canadian and Russian Arctic, and Svalbard (Figure 6). Important volumes are also found for Alaska (51 mm SLE), High Mountain Asia (24 mm), and the South American Andes (17 mm). Our results are backed up with

Table 1. Sensitivity of Total Ice Volume (All RGI Glaciers) to Variations in Five Parameters Deemed to Be Important[a]

Parameter	Range	Unit	ΔV (%)
$\widetilde{db}/dz_{abl,0}$	0.004/**0.007**	mwe m^{-1}	−3.8/+5.3
S_{crit}	**10**/40	km^2	+0.5/−0.7
f_{cont}	1600/**3200**	m	−1.5/+2.2
A_f (T = 0)	**0.06**/0.09	bars^{-3} yr^{-1}	+3.3/−5.4
Δ ELA$_{calv}$	−100/+**100**	m	−1.8/+2.9

[a]The parameter values yielding a larger ice volume are printed in bold. Differences in calculated global ice volume ΔV relative to the reference parameter set (see Table S2 in Text S1) are given in percent.

thickness observations from almost 300 glaciers across all regions (Table 2 and Figure 5).

[34] We compute a global glacier ice volume 30% lower than the estimate by *Radić and Hock* [2010]. The error bars do not overlap. Comparison excluding glaciers around Greenland and Antarctica indicates volumes 13% below those obtained by *Dyurgerov and Meier* [2005], and 18% and 15% above estimates by *Raper and Braithwaite* [2005] and *Ohmura* [2010], respectively.

[35] In order to assess the differences compared to previous studies that were exclusively based on volume-area scaling, we also calculate ice volume using the relation

$$\overline{h} = cS^{\gamma}, \tag{8}$$

with $\overline{h}$ the mean thickness in m, S the glacier area in m^2, and the constants c and γ [e.g., *Macheret et al.*, 1988; *Bahr et al.*, 1997]. For consistency, we use the same parameters as [*Radić and Hock*, 2010] who have defined two separate scaling relations for mountain glaciers (c = 0.2055, γ = 0.375) and for ice caps (c = 1.7026, γ = 0.250). As no information whether a glacier shape is a mountain glacier or an ice cap is provided by the RGI, we define a region-specific size threshold (see Figure 7). Our global glacier ice volume is 8% below that calculated using volume-area scaling based on areas from the RGI. Our regional volumes differ from those obtained by volume-area scaling by between −63% (central Asia) and +35% (Arctic Canada South) (Table 2). Differences for individual glaciers can be even higher. This indicates that glacier volume estimates using scaling approaches might be subject to significant local and regional biases that can be crucial in projecting the future impacts of glacier changes.

[36] In general, we find systematically lower volumes for large glaciers compared to volume-area scaling (Figure 7). Although these glaciers contain most of the ice, scaling relations are poorly constrained for this size class due to a lack of thickness measurements. The presence of glacier complexes in the RGI further explains some of the differences between our estimates and those obtained by volume-area scaling. Tests for the RGI region Arctic Canada South show that the volume computed based on equation (8) increases by 71% when individual glacier outlines are not separated, i.e., when glacier complexes are present. The sensitivity of our approach to this imperfection in glacier inventory data is much smaller (<10%). This indicates that a comparison of our results to volume-area scaling (see Table 2) might be biased in regions where glacier complexes are present in the RGI.

[37] The important regional differences of our results compared to statistical scaling (Table 2) indicate that a single scaling relation might not be valid for the entire globe. Therefore, we derive region-specific thickness-area scaling functions (equation (8)) using the physically based ice volume estimates for 171,000 glaciers worldwide (Figure 7). Exponents γ are lower than previously published values [e.g., *Chen and Ohmura*, 1990; *Bahr et al.*, 1997]. This might be explained by the unsuitability of conventional

Table 2. Calculated Total Ice Volume and Validation Data for 19 Regions[a]

Region	n	S (km^2)	V (km^3)	$\overline{h}$ (m)	SLE (mm)	$n(h_{avg})$	$\Delta\overline{h_{avg}}$ (m)	$n(h_p)$	$\Delta\overline{h_p}$ (m)	ΔV_{sc} (%)
Alaska	22,916	89,901	20,402 ± 1,501	226	50.7 ± 3.7	2	23	7	57	−29
Antarctic and Subantarctic	3,318	133,173	37,517 ± 8,402	281	93.1 ± 20.9	2	−48	4	−86	−11
Arctic Canada North	3,205	105,139	34,399 ± 4,699	327	85.4 ± 11.7	0	0	2	71	26
Arctic Canada South	6,679	40,893	9,814 ± 1,115	240	24.4 ± 2.8	1	91	0	0	35
Caucasus and Middle East	1,335	1,121	61 ± 6	55	0.2 ± 0.0	0	0	2	−38	−10
Central Asia	30,131	64,448	5,026 ± 503	77	12.5 ± 1.2	43	−11	6	−14	−63
Central Europe	3,888	2,060	117 ± 10	56	0.3 ± 0.0	40	4	25	−14	−15
Greenland Periphery	13,860	87,765	19,042 ± 2,655	216	47.3 ± 6.6	1	−14	1	36	−14
Iceland	289	11,055	4,441 ± 370	401	11.0 ± 0.9	1	8	2	0	4
Low Latitudes	4,979	4,074	144 ± 16	35	0.4 ± 0.0	0	0	1	−38	−42
New Zealand	3,002	1,160	70 ± 5	60	0.2 ± 0.0	0	0	2	−33	−49
North Asia	3,455	2,816	140 ± 15	49	0.3 ± 0.0	62	−16	0	0	−35
Russian Arctic	353	51,665	16,839 ± 2,205	325	41.8 ± 5.5	14	39	2	31	3
Scandinavia	1,795	2,846	256 ± 19	90	0.6 ± 0.0	5	−34	5	−35	−45
South Asia East	13,615	21,699	1,312 ± 119	60	3.3 ± 0.3	2	25	3	15	−30
South Asia West	22,563	33,961	3,241 ± 287	95	8.0 ± 0.7	0	0	1	1	−31
Southern Andes	19,089	32,521	6,674 ± 507	205	16.6 ± 1.3	0	0	4	−3	−4
Svalbard	2,058	33,932	9,685 ± 922	285	24.0 ± 2.3	25	21	18	83	31
Western Canada and USA	14,516	14,615	1,025 ± 84	70	2.5 ± 0.2	20	7	2	−40	−19
Total	171,046	734,856	170,214 ± 20,688	231	422.6 ± 57.1	218	0	87	10	−8

[a]The number n of evaluated glaciers, the total area S according to the RGI, the calculated volume V, mean ice thickness $\overline{h}$ and the corresponding sea level equivalent SLE are given. Calculated thickness is compared to $n(h_{avg})$ glaciers with mean thickness data and $n(h_p)$ glaciers with point measurements. The regional biases $\Delta\overline{h_{avg}}$ and $\Delta\overline{h_p}$ are stated. ΔV_{sc} is the relative difference in ice volume as calculated here minus that obtained by volume-area scaling using the RGI data and the parameters from *Radić and Hock* [2010].

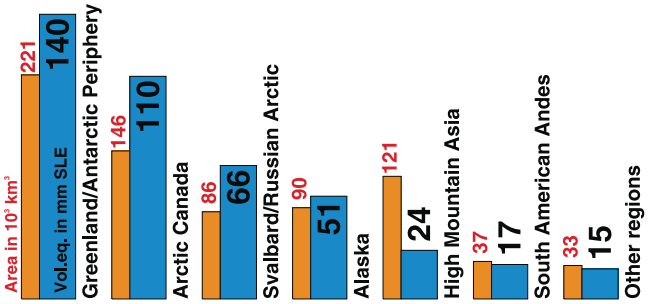

Figure 6. Regional distribution of glacier area (orange) according to the RGI v2.0 in 10^3 km^2, and calculated sea level rise potential (blue) in mm SLE.

scaling relations for nonsteady state and/or markedly dendritic glaciers.

6. Conclusion

[38] Based on complete glacier inventory data and terrain elevation models the ice thickness distribution and volume of all glaciers and ice caps around the globe has been calculated. A new approach for the inversion of distributed ice thickness from surface topography using readily available input data is applied, providing the first physically based global ice volume estimate that accounts for the characteristics of each individual glacier. We find an ice volume outside of the two ice sheets of $170 \times 10^3 \pm 21 \times 10^3$ km^3, or 0.43 ± 0.06 m SLE, which is below previous estimates.

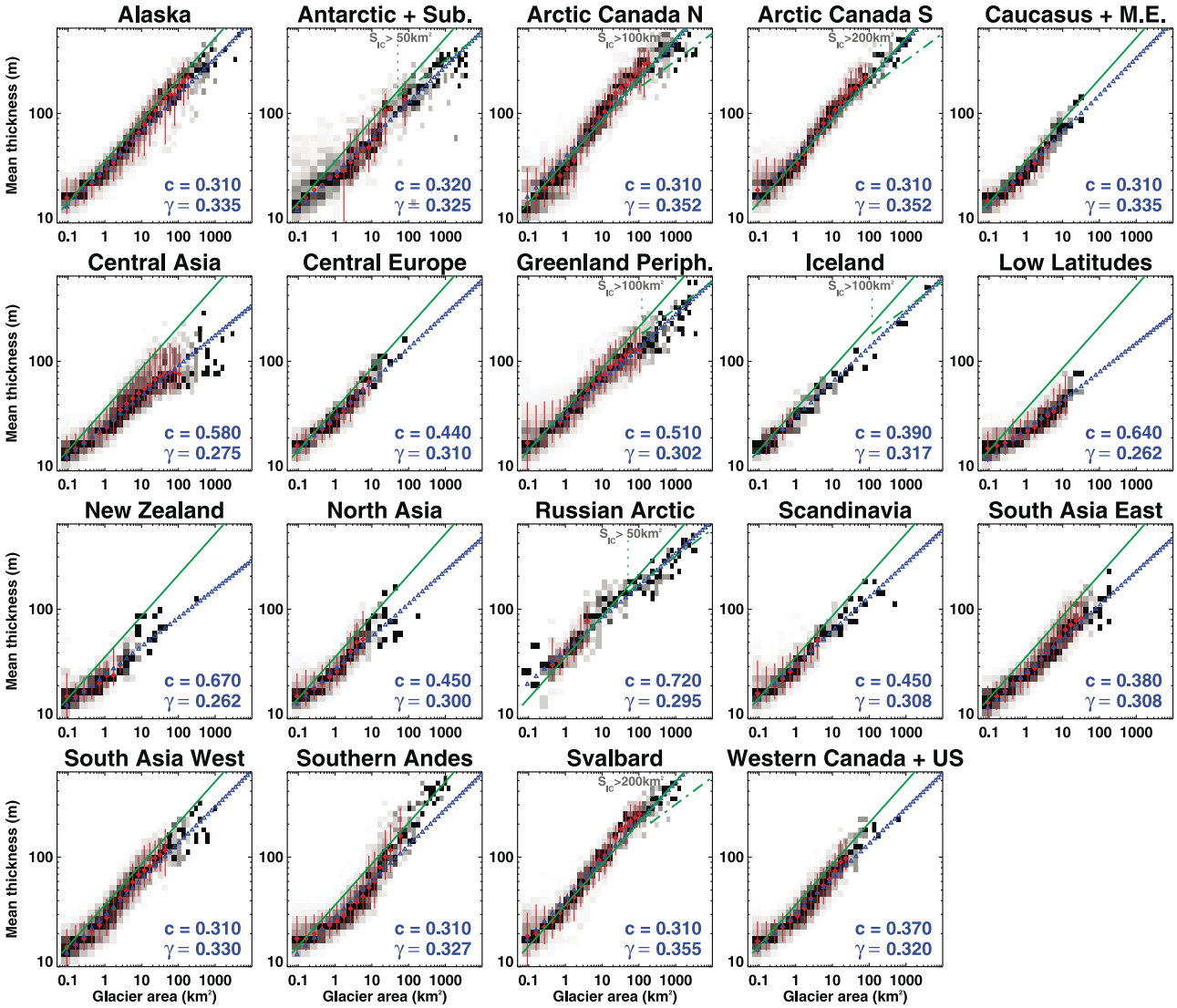

Figure 7. RGI glacier area versus calculated ice thickness for all regions. Note that both axes are logarithmic. Gray scales depict relative point density (calculated ice thickness of individual glaciers) in glacier size bins. For classes with more than 20 glaciers, red bars indicate the 10% and 90% quantiles, the diamond refers to the median. Blue triangles show the best fit of a region-specific thickness-area scaling relation. Optimized parameters according to equation (8) are given. The solid green line (mountain glaciers) and dash-dotted line (ice caps) show thickness based on the volume-area scaling relations used by *Radić and Hock* [2010]. Size thresholds S_{IC} between glaciers and ice caps are assumed to be constant for each region.

The uncertainties in this new global ice volume assessment are however still considerable. A further homogenization of glacier inventory data and an extended data set of direct thickness observations would be among the requirements for reducing them.

[39] We derive spatially distributed ice thickness estimates for 171,000 glaciers from ice dynamical considerations and provide a detailed view on regional to single-glacier scales of fresh water resources and the sea level rise potential of mountain regions. Our results form the basis for a more accurate assessment of changes in the hydrological regime of glacierized basins, and the future contribution of melting glaciers and ice caps to global sea level rise.

[40] **Acknowledgments.** We thank all scientists contributing to the Randolph Glacier Inventory. SRTM DEMs were provided by CGIAR-CSI, and ASTER DEMs by NASA. J. G. Cogley and R. Hock are acknowledged for contributing previous compilations of observed ice thickness data. Helpful comments by A. Arendt, J. G. Cogley and an anonymous reviewer improved the manuscript.

References

Arendt, A., et al. (2012), Randolph Glacier Inventory: A Dataset of Global Glacier Outlines, version 2.0, digital media, http://www.glims.org/RGI/RGI_Tech_Report_V2.0.pdf, Global Land Ice Measure. from Space, Boulder, Colo.

Azam, M. F., et al. (2012), From balance to imbalance: A shift in the dynamic behaviour of Chhota Shigri glacier, western Himalaya, India, *J. Glaciol.*, *58*(208), 315–324, doi:10.3189/2012JoG11J123.

Bahr, D. B., M. F. Meier, and S. D. Peckham (1997), The physical basis of glacier volume-area scaling, *J. Geophys. Res.*, *102*(B9), 20,355–20,362, doi:10.1029/97JB01696.

Chen, J., and A. Ohmura (1990), Estimation of Alpine glacier water resources and their change since the 1870s, in *Hydrology in Mountainous Regions I*, *IAHS-AISH Publ.*, *193*, 127–135.

Clarke, G. K. C., E. Berthier, C. G. Schoof, and A. H. Jarosch (2009), Neural networks applied to estimating subglacial topography and glacier volume, *J. Clim.*, *22*, 2146–2160, doi:10.1175/2008JCLI2572.1.

Cogley, J. G. (2012), The future of the world's glaciers, in *The Future of the World's Climate*, 2nd ed., edited by A. Henderson-Sellers and K. McGuffie, pp. 197–222, Elsevier, Amsterdam.

Cogley, J. G., et al. (2011), *Glossary of Glacier Mass Balance and Related Terms*, *IHP-VII Tech. Doc. Hydrol.*, vol. 86, UNESCO, Paris.

Cuffey, K. M., and W. S. B. Paterson (2010), *The Physics of Glaciers*, 4th ed., 704 pp., Butterworth-Heinemann, Oxford, U. K.

Dowdeswell, J. A., et al. (2002), Form and flow of the Academy of Sciences Ice Cap, Severnaya Zemlya, Russian High Arctic, *J. Geophys. Res.*, *107*(B4), 2076, doi:10.1029/2000JB000129.

Dyurgerov, M. B., and M. F. Meier (2005), Glaciers and the changing Earth system: A 2004 snapshot, *Occas. Pap. 58*, 117 pp., Inst. of Arct. and Alp. Res., Univ. of Colo. at Boulder, Boulder.

Farinotti, D., M. Huss, A. Bauder, and M. Funk (2009a), An estimate of the glacier ice volume in the Swiss Alps, *Global Planet. Change*, *68*(3), 225–231.

Farinotti, D., M. Huss, A. Bauder, M. Funk, and M. Truffer (2009b), A method for estimating the ice volume and ice thickness distribution of alpine glaciers, *J. Glaciol.*, *55*(191), 422–430.

Frey, H., and F. Paul (2012), On the suitability of the SRTM DEM and ASTER GDEM for the compilation of topographic parameters in glacier inventories, *Int. J. Appl. Earth Obs. Geoinf.*, *18*, 480–490, doi:10.1016/j.jag.2011.09.020.

Fujita, K., R. Suzuki, T. Nuimura, and A. Sakai (2008), Performance of ASTER and SRTM DEMs, and their potential for assessing glacial lakes in the Lunana region, Bhutan Himalaya, *J. Glaciol.*, *54*, 220–228.

Glen, J. W. (1955), The creep of polycrystalline ice, *Proc. R. Soc. London*, *228*(1175), 519–538.

Gudmundsson, G. H. (1999), A three-dimensional numerical model of the confluence area of Unteraargletscher, Bernese Alps, Switzerland, *J. Glaciol.*, *45*(150), 219–230.

Haeberli, W., and M. Hoelzle (1995), Application of inventory data for estimating characteristics of and regional climate-change effects on mountain glaciers: A pilot study with the European Alps, *Ann. Glaciol.*, *21*, 206–212.

Hagen, J. O., K. Melvold, F. Pinglot, and J. A. Dowdeswell (2003), On the net mass balance of the glaciers and ice caps in Svalbard, Norwegian Arctic, *Arct. Antarct. Alp. Res.*, *35*, 264–270.

Hoelzle, M., W. Haeberli, M. Dischl, and W. Peschke (2003), Secular glacier mass balances derived from cumulative glacier length changes, *Global Planet. Change*, *36*(4), 295–306.

Huang, M. (1990), On the temperature distribution of glaciers in China, *J. Glaciol.*, *36*(123), 210–216.

Jarvis, J., H. Reuter, A. Nelson, and E. Guevara (2008), Hole-filled SRTM for the globe, CGIAR-CSI SRTM 90 m Database, Version 4, http://srtm.csi.cgiar.org/, CGIAR Consort. for Spatial Inf., Montpellier, France.

Jóhannesson, T., C. Raymond, and E. Waddington (1989), Time-scale for adjustment of glaciers to changes in mass balance, *J. Glaciol.*, *35*(121), 355–369.

Kalnay, E., et al. (1996), The NCEP/NCAR 40-Year Reanalysis Project, *Bull. Am. Meteorol. Soc.*, *77*, 437–472.

Kamb, B., and K. A. Echelmeyer (1986), Stress-gradient coupling in glacier flow: I. Longitudinal averaging of the influence of ice thickness and surface slope, *J. Glaciol.*, *32*, 267–284.

Li, H., F. Ng, Z. Li, D. Qin, and G. Cheng (2012), An extended "perfect-plasticity" method for estimating ice thickness along the flow line of mountain glaciers, *J. Geophys. Res.*, *117*, F01020, doi:10.1029/2011JF002104.

Linsbauer, A., F. Paul, and W. Haeberli (2012), Modeling glacier thickness distribution and bed topography over entire mountain ranges with GlabTop: Application of a fast and robust approach, *J. Geophys. Res.*, *117*, F03007, doi:10.1029/2011JF002313.

Macheret, Y., P. Cherkasov, and L. Bobrova (1988), Tolshchina i ob'em lednikov Dzhungarskogo Alatau po dannym aeroradiozondirovaniya, *Mater. Glyatsiologicheskikh Issled.*, *62*, 60–71.

Meier, M. F., M. B. Dyurgerov, U. K. Rick, S. O'Neel, W. T. Pfeffer, R. S. Anderson, S. P. Anderson, and A. F. Glazovsky (2007), Glaciers dominate eustatic sea-level rise in the 21st century, *Science*, *317*(5841), 1064–1067, doi:10.1126/science.1143906.

Nolan, M., R. J. Motyka, K. Echelmeyer, and D. C. Trabant (1995), Ice-thickness measurements of Taku Glacier, Alaska, U.S.A., and their relevance to its recent behavior, *J. Glaciol.*, *41*, 541–553.

Nye, J. F. (1965), The flow of a glacier in a channel of rectangular, elliptic or parabolic cross-section, *J. Glaciol.*, *5*(41), 661–690.

Oerlemans, J., and J. P. F. Fortuin (1992), Sensitivity of glaciers and small ice caps to greenhouse warming, *Science*, *258*(5079), 115–117, doi:10.1126/science.258.5079.115.

Ohmura, A. (2010), Completing the World Glacier Inventory, *Ann. Glaciol.*, *50*(53), 144–148.

Paterson, W. S. B. (1970), The sliding velocity of Athabasca Glacier, Canada, *J. Glaciol.*, *9*, 55–63.

Radić, V., and R. Hock (2010), Regional and global volumes of glaciers derived from statistical upscaling of glacier inventory data, *J. Geophys. Res.*, *115*, F01010, doi:10.1029/2009JF001373.

Radić, V., and R. Hock (2011), Regionally differentiated contribution of mountain glaciers and ice caps to future sea-level rise, *Nat. Geosci.*, *4*, 91–94, doi:10.1038/ngeo1052.

Raper, S. C. B., and R. J. Braithwaite (2005), The potential for sea level rise: New estimates from glacier and ice cap area and volume distributions, *Geophys. Res. Lett.*, *32*, L05502, doi:10.1029/2004GL021981.

Rastner, P. N., T. Mölg, H. Machguth, and F. Paul (2012), The first complete glacier inventory for the whole of Greenland, *Cryosphere Discuss.*, *6*(4), 2399–2436.

Raup, B., A. Racoviteanu, S. J. S. Khalsa, C. Helm, R. Armstrong, and Y. Arnaud (2007), The GLIMS geospatial glacier database: A new tool for studying glacier change, *Global Planet. Change*, *56*, 101–110.

World Glacier Monitoring Service (WGMS) (2008), Fluctuations of Glaciers, 2000–2005, vol. IX, http://www.geo.uzh.ch/microsite/wgms/fog.html, Zurich, Switzerland.

Williamson, S., M. Sharp, J. Dowdeswell, and T. Benham (2008), Iceberg calving rates from northern Ellesmere Island ice caps, Canadian Arctic, 1999–2003, *J. Glaciol.*, *54*, 391–400, doi:10.3189/002214308785837048.